TReATS: A novel method for TAT-Cre Recombinase-mediated floxed Allele modification in *ex vivo* Tissue Slices

Sek-Shir Cheong[1], Tiago C. Luis[2], Michelle Stewart[3], Rosie Hillier[3], Matthew Hind[1,4], Charlotte H. Dean[1,*]

[1]National Heart and Lung Institute (NHLI), Imperial College London, London SW7 2AZ, UK
[2]Centre for Inflammatory Diseases, Department Immunology and Inflammation, Imperial College London, London W12 N00, UK
[3]The Mary Lyon Centre at MRC Harwell, Harwell Campus, Oxfordshire, OX11 0RD, UK
[4]National Institute for Health Research (NIHR) Respiratory Biomedical Research Unit at the Royal Brompton & Harefield NHS Foundation Trust, London SW3 6NP, UK

*Correspondence: Dr Charlotte Dean, NHLI, Imperial College London, London SW7 2AZ, UK (ORCID: 0000-0002-8846-5472)
Email: c.dean@imperial.ac.uk

Keywords: TAT-Cre, cell-permeant Cre recombinase, allele modification, gene manipulation, precision-cut lung slices, precision-cut tissue slices

Abstract

Precision-Cut Lung Slices (PCLS) are used for a variety of applications. However, methods to manipulate genes in PCLS are currently limited. We developed a novel method, TAT-Cre Recombinase-mediated floxed Allele modification in Tissue Slices (TReATS), to induce highly effective and temporally controlled gene deletion or activation in *ex vivo* PCLS. Treatment of PCLS from *Rosa26-flox-stop-flox-EYFP* mice with cell-permeant TAT-Cre recombinase induced ubiquitous EYFP protein expression, indicating successful Cre-mediated excision of the upstream *loxP*-flanked stop sequence. Quantitative real-time PCR confirmed induction of *EYFP*. We successfully replicated the TReATS method in PCLS from *Vangl2*$^{flox/flox}$ mice, leading to the deletion of *loxP*-flanked exon 4 of the *Vangl2* gene. Cre-treated *Vangl2*$^{flox/flox}$ PCLS exhibited cytoskeletal abnormalities, a known phenotype caused by VANGL2

dysfunction. We report a novel method that by-passes conventional Cre-Lox breeding, allowing rapid and highly effective gene manipulation in *ex vivo* tissue models.

INTRODUCTION

Precision-Cut Tissue Slices (PCTS) are an established *ex vivo* method of culturing 3D tissue slices of uniform thickness derived from human or animal organs. The use of tissue slices was first introduced in the early 20th century. However, the original model had major limitations due to the lack of slicing devices, vibrating microtomes, and suboptimal incubation methods, which led to inconsistent size, thickness and viability of slices (Majorova et al., 2021). These limitations improved following the development of the Krumdieck tissue slicer (Krumdieck et al., 1980), which enables tissue to be cut at a precise, pre-defined thickness.

The PCTS technique has been applied to produce slices from different organs, including heart (Ou et al., 2020), brain (Pai and Ravindranath, 1991), kidney (De Kanter et al., 2004), liver and intestine (De Graaf et al., 2010). Using the precision cutting technique, a large number of slices can be generated from an organ, allowing the study of a wide range of conditions or variables whilst greatly reducing the experimental time, costs and tissue resources required. PCTS retain the overall anatomical architecture and composition of the *in vivo* organ including appropriate cell:cell contacts, ratios and cell-extracellular matrix interactions whereas other models, such as organoids or organ-on-a-chip, do not recapitulate the cellular and spatial complexity of the intact organ. Given the advantages of PCTS, they have become a popular 3D model that bridges the gap between *in vitro* and *in vivo* systems.

The protocols used to prepare PCTS from different organs are similar with only slight modifications depending on the organ consistency and species used. For example, generation of precision-cut lung slices (PCLS) requires introduction of agarose into the airways to provide structural support and maintain the fragile architecture of lung tissue, during and after slicing (Placke and Fisher, 1987). In this study, we focused on lung slices, which are now routinely used for a variety of applications, including disease modelling (Alsafadi et al., 2017), drug toxicology studies (Närhi et al., 2018), host-pathogen interaction investigations (Bryson et al., 2020), injury and repair studies (Kim et al., 2021), and for live imaging to visualise dynamic cellular behaviour

in real-time (Akram et al., 2019a). Despite the broad range of applications for which PCTS are now used, methods to manipulate genes in tissue slices remain very limited.

PCLS consist mainly of the parenchyma (gas exchanging portion of the lungs) as well as some small airways. Within the parenchyma there are many alveoli, each of which is comprised of a layer of epithelial cells adjacent to a capillary network, enabling efficient gaseous diffusion. Although there are numerous different cell types in the adult lung parenchyma, the three key cell types that form the alveoli are endothelial cells that form the fine capillary tubes and two epithelial sub-types, alveolar type 1 and type 2 cells (AT1 and AT2) from which the alveolar walls are built (Guillot et al., 2013). In addition, lung fibroblasts and macrophages are integral components of the lung parenchyma. Lung fibroblasts produce extracellular matrix (ECM) components to support lung structure and function, as well as playing a pivotal role in orchestrating lung repair and remodelling in response to injury (White, 2015). Macrophages are key innate immune cells within the lungs that safeguard the respiratory system by helping to control the immune response against pathogens and foreign particles (Byrne et al., 2015).

Cre-Lox technology has been used extensively to generate conditional alleles and is a powerful system for introducing different types of genetic alteration: deletion, inversion, insertion, and translocation, depending on the orientation of the *loxP* sites on the modified alleles (Branda and Dymecki, 2004). The Cre enzyme is used to drive the recombination of generated floxed alleles. Different methods are available to facilitate Cre expression that allows spatial or temporal control of conditional mutagenesis, including breeding with a Cre transgenic mouse, induction of modified Cre, CreERT2, by tamoxifen or 4-hydroxy-tamoxifen (4OH-T) administration (Savery et al., 2020), transfection or viral transduction of DNA plasmid encoding Cre protein (Geoffroy and Raineteau, 2007; Rohlmann et al., 1996), and delivery of Cre mRNA (Kauffman et al., 2018). A more recently developed method employs protein-transduction domains (PTDs) such as TAT peptide derived from HIV-TAT and a nuclear localisation sequence (NLS) fused with the biologically active Cre protein to facilitate cell permeability (Peitz et al., 2002).

Cell-permeant Cre recombinase and other aforementioned Cre delivery methods have been used to successfully induce DNA recombination across different experimental settings, including cell monolayer cultures, embryo explants, including

whole embryonic lungs, and restricted regions of central nervous system tissue (Gitton et al., 2009; Morimoto et al., 2010; Peitz et al., 2002; Ryder et al., 2014; Savery et al., 2020). Given the versatility and uniformity of PCTS compared to organotypic explants, we hypothesised that the administration of cell-permeant TAT-Cre recombinase might be an effective method for *ex vivo* genetic manipulation in PCTS derived from floxed animals (floxed-PCTS) of any age, including adult.

Here we demonstrate for the first time that TAT-Cre can effectively induce recombination of *loxP*-modified alleles without the requirement of a Cre allele, leading to successful gene activation or deletion in *ex vivo* PCLS. The TReATS (TAT-Cre Recombinase-mediated floxed Allele modification in Tissue Slices) method obviates the need for complex breeding strategies to generate animal models of interest. We anticipate this method will be widely applicable to PCTS from other organs and will expedite the discovery of gene function, disease mechanisms and potential therapeutics.

RESULTS

Highly efficient TAT-Cre recombinase-mediated transgene activation in *R26R-EYFP* mouse PCLS

We first tested TAT-Cre recombinase in PCLS generated from homozygous *Rosa26-flox-stop-flox-EYFP* reporter mice (abbreviated as *R26R-EYFP* hereafter). *R26R-EYFP* reporter mice have a *loxP*-flanked stop sequence localised upstream of an enhanced yellow fluorescent protein (*EYFP*) gene inserted into the ubiquitously expressed *Gt(ROSA)26Sor* locus. In the absence of Cre recombinase activity, the transcription of *EYFP* gene is suppressed by the upstream stop codon. Upon exposure to Cre recombinase, the stop sequence is excised, allowing the expression of EYFP protein, which can readily be visualised under a fluorescence microscope (Fig. 1A).

PCLS from *R26R-EYFP* were incubated with 3 µM of TAT-Cre recombinase in serum-free (SF) Dulbecco's Modified Eagle Medium (DMEM) culture media. At 72 h post-incubation, ubiquitous expression of EYFP protein was observed across PCLS (Fig. 1B), indicating successful deletion of the stop sequence upstream of the *EYFP* gene (Fig. 1A). PCLS from the same mouse cultured without TAT-Cre were used as a negative control; no EYFP was visible in these PCLS (Fig. 1C). To further validate these observations, quantitative real-time PCR (qRT-PCR) was performed on cDNA

obtained from PCLS. There was approximately a 70-fold increase in *EYFP* transcript levels ($p = 0.0286$) in TAT-Cre recombinase-treated PCLS, compared to *R26R-EYFP* PCLS cultured without TAT-Cre (negative control), where *EYFP* was undetected (Fig. 1D).

To assess whether TAT-Cre affects the viability of PCLS, MTT (3-[4,5-dimethylthiazol-2-yl]-2,5-diphenyltetrazolium bromide) assays were conducted. TAT-Cre treatment did not result in a significant change in metabolic activity (0.99) compared to untreated, control PCLS (1.00). In contrast, PCLS treated with 70% methanol, a positive control for dead cells, showed minimal metabolic activity (0.10 vs 1.00 in untreated control PCLS; $p = 0.0096$) (Fig. 1E).

Furthermore, to determine whether TAT-Cre recombinase can penetrate throughout the whole tissue slice, confocal imaging was used to obtain Z-stacks, reaching a depth of 125 µm, which corresponds to the midpoint of a 250-µm-thick slice. Notably, EYFP expression was present throughout the Z-stacks, indicating efficient penetrance of TAT-Cre recombinase and subsequent activation of the *EYFP* gene through the entire thickness of PCLS (Movie S1).

TAT-Cre recombinase-mediated *EYFP* activation in key alveolar cell types within PCLS

To identify in which alveolar cell types TAT-Cre recombinase-mediated EYFP activation occurs, TAT-Cre treated *R26R-EYFP* PCLS were immunolabelled with conjugated antibodies against previously characterised alveolar cell type-specific markers: lysosomal associated membrane protein 3 (LAMP3) for mature differentiated AT2 cells (Laresgoiti et al., 2016), podoplanin (PDPN) for AT1 cells (Marconett et al., 2017), platelet endothelial cell adhesion molecule (PECAM) for the vascular endothelium (DeLisser et al., 2006), vimentin for fibroblast cells (Surolia et al., 2019), and CD11c for macrophages (Misharin et al., 2013). EYFP was present in each of these cell-types (Fig. 2A-E), demonstrating that TAT-Cre recombinase treatment effectively induced *EYFP* gene activation in multiple alveolar cell populations within PCLS.

TAT-Cre recombinase-mediated *Vangl2* deletion in *Vangl2*$^{flox/flox}$ mouse PCLS

Next, to show proof-of-principle that TAT-Cre could be used to drive recombination in a different floxed system, PCLS from homozygous adult *Vangl2*$^{flox/flox}$ mice were obtained to test whether TAT-Cre recombinase could be used to delete a gene of

interest in tissue slices. We chose *Vangl2*^{flox} mice because VANGL2 is known to regulate actin cytoskeleton remodelling (Poobalasingam et al., 2017; Yates et al., 2010; Zhang et al., 2020). We reasoned that if successful, the deletion of *Vangl2* would result in visible disruption to filamentous actin (F-actin) organisation, a phenotype that could readily be detected.

The *Vangl2*^{flox} allele is illustrated in Figure 3A; *loxP* sites flank exon 4 of the *Vangl2* gene. Upon exposure to Cre, recombination between the *loxP* sites results in excision of exon 4, leading to the introduction of a premature stop codon that gives rise to a truncated protein lacking the crucial trans-membrane domains and a C-terminal PDZ-binding domain that is required for interaction with other binding partners (Ramsbottom et al., 2014) (Fig. 3A). To test whether TAT-Cre could mediate recombination of the *Vangl2*^{flox} allele in *ex vivo* culture, PCLS generated from a homozygous adult *Vangl2*$^{flox/flox}$ mouse were incubated with 5 µM of TAT-Cre recombinase. After 72 h in culture, total RNA was extracted and qRT-PCR was performed using primers spanning exon 3-4 boundary of the *Vangl2* gene. Results from the qRT-PCR demonstrated a significant 70% reduction ($p<0.001$) in transcript levels of *Vangl2* in TAT-Cre recombinase-treated PCLS compared with that of untreated, control PCLS from the same mouse, indicating successful TAT-Cre recombinase-mediated excision of floxed exon 4 (Fig. 3B). MTT assays demonstrated that metabolic activity in PCLS treated with 5 µM of TAT-Cre recombinase was not significantly different from untreated, control PCLS (0.80 in Cre-treated PCLS vs 1.00 in control PCLS), indicating that cell viability was sufficiently maintained (Fig. 3C). Methanol-treated PCLS showed a significant reduction in metabolic activity as expected (0.09 vs 1.00 in untreated, control PCLS; $p<0.05$) (Fig. 3C).

Phenotypic characterisation of TAT-Cre-treated *Vangl2*$^{flox/flox}$ PCLS

VANGL2 is a core component of the planar cell polarity (PCP) pathway. This pathway plays a key role in driving tissue morphogenesis and repair by regulating actin cytoskeleton organisation (Poobalasingam et al., 2017; Yates et al., 2010; Zhang et al., 2020). Loss of functional VANGL2 protein is known to disrupt embryonic lung branching, alveologenesis, and adult lung repair following injury, due to dysfunctional actomyosin-driven cell migration (Cheong et al., 2020; Poobalasingam et al., 2017; Yates et al., 2010). Thus, one of the prominent phenotypes that results from VANGL2 dysfunction is highly disrupted F-actin organisation, as previously

shown in a number of studies using the *Vangl2* loss-of-function (LOF) allele, *Looptail (Vangl2^{Lp})* (Cheong et al., 2020; Poobalasingam et al., 2017; Yates et al., 2010).

To investigate whether TAT-Cre recombinase-mediated *Vangl2* deletion in *Vangl2$^{flox/flox}$* PCLS led to similar aberrant F-actin organisation defects, PCLS were cultured for 72 h with or without TAT-Cre and then labelled with Rhodamine Phalloidin. As expected, untreated, control PCLS from *Vangl2$^{flox/flox}$* mice exhibited normal F-actin distribution (Fig. 3D; yellow). In contrast, F-actin was severely disrupted in *Vangl2$^{flox/flox}$* PCLS treated with 5 µM TAT-Cre recombinase (Fig. 3E; yellow). Notably this phenotype was more profound than that in PCLS from adult heterozygous *Vangl2$^{Lp/+}$* mutants (Fig. 3F; yellow). Homozygous *Vangl2$^{Lp/Lp}$* mice are not viable beyond perinatal stage, precluding any comparison between Cre-treated *Vangl2$^{flox/flox}$* PCLS with that of adult homozygous *Vangl2$^{Lp/Lp}$*.

VANGL2 dysfunction has previously been shown to hamper traction force generation and mechanosignalling due to defects in actomyosin contractility (Cheong et al., 2020). Perturbation of cytoplasmic intermediate filaments (IFs) is also known to impact mechanical integrity, causing reduced cell stiffness (Sanghvi-Shah and Weber, 2017). This prompted us to speculate that *Vangl2* deletion may also affect IFs. To investigate the effect of *Vangl2* deletion on IFs, Cre-treated and untreated, control *Vangl2$^{flox/flox}$* PCLS were immunostained with pan-cytokeratin, a marker for epithelial cell IFs. Interestingly, Cre-treated *Vangl2$^{flox/flox}$* PCLS displayed highly aberrant IFs (Fig. 3E; magenta) compared with untreated, control PCLS from the same mouse (Fig. 3D; magenta), indicating that loss of VANGL2 perturbed IF distribution. Notably, similar, albeit less severe, abnormalities in IFs were also observed in heterozygous *Vangl2$^{Lp/+}$* PCLS (Fig. 3F; magenta).

To confirm that the observed phenotypes in F-actin and IFs were a consequence of *Vangl2* disruption rather than arising from adverse effects of TAT-Cre recombinase, the same dosage of TAT-Cre recombinase was used to treat PCLS from wild-type mice. Figure 4A shows the presence of normal F-actin (yellow) and IFs (magenta) in untreated PCLS from wild-type mice, which were indistinguishable from wild-type PCLS treated with 5 µM of TAT-Cre recombinase (Fig. 4B). This finding indicates that F-actin and IF anomalies observed in TAT-Cre recombinase-treated *Vangl2$^{flox/flox}$* PCLS were due to the loss of functional VANGL2 protein and were not a result of toxic or off-target effects from exogenous Cre treatment.

DISCUSSION

Precision-Cut Lung Slices (PCLS) are an invaluable *ex vivo* model that closely recapitulates the complexity of the native lung environment (Alsafadi et al., 2020). While *in vivo* models offer greater biological relevance, data generated from *in vivo* studies are often complex to interpret due to the presence of multiple variables. Moreover, the number of animals required for *in vivo* experiments is considerable with associated ethical and financial implications. PCLS, on the contrary, serve as an excellent intermediate model bridging the gap between *in vitro* and *in vivo* models. However, until now, a major limitation of tissue slice models has been the lack of effective methods for genetic manipulation within *ex vivo* tissue. Currently, the only established genetic modification method for PCLS involves gene silencing through passive transfection of small interfering RNA (siRNA), which comes with drawbacks such as transient gene silencing effects and low transfection efficiency (Ruigrok et al., 2017). Thus, the development of a technique allowing permanent and irreversible gene deletion or activation within PCLS greatly enhances the versatility of this model, broadening the spectrum of studies that will be feasible with this platform.

Previously, several methods have been employed to induce Cre-mediated recombination of *loxP*-modified alleles. However, each of these methods has its limitations such as leakiness of the Cre system *in vitro* or *in vivo* (Fuhrmann-Benzakein et al., 2000), costly and laborious breeding strategies, risk of toxicity caused by Cre inducing agents such as 4OH-T (Denk et al., 2015; Savery et al., 2020), low transfection efficiencies of Cre plasmids or mRNA resulting in low recombination, instability of mRNA (Bugeon et al., 2017; Van Den Plas et al., 2003), and insertional mutagenesis caused by viral transduction (Peitz et al., 2002).

To overcome these issues, this study demonstrates a novel approach using cell-permeant TAT-Cre recombinase for efficient *loxP*-modified allele modification in adult *ex vivo* 3D tissue slices, TReATS (Fig. 5).

This method offers several advantages. Firstly, Cre protein administration in PCLS by-passes complex crossbreeding strategies involving Cre transgenic mice, considerably reducing the number of animals required for experiments, in line with the 3Rs principles (Replacement, Refinement and Reduction of animals in research) (Hubrecht and Carter, 2019) as well as greatly reducing experimental time and cost.

Secondly, it provides a rapid solution to overcome the issue of embryonic or perinatal lethality. Mice carrying LOF allele(s) of genes required for development often die at or around birth. For example, homozygous LOF mutants of *Vangl2* (and other PCP pathway genes such as *Wnt5a* and *Ror2*) die *in utero* or perinatally due to severe neural tube defects (Oishi et al., 2003; Yates et al., 2010; Yin et al., 2012), limiting studies in adulthood to heterozygous mutants only. In cases where a gene plays a critical role in the function of a vital organ or system, even conditional gene deletion within specific cell populations may not prevent lethality. Conditional deletion of *Vangl2, Wnt5a* or *Ror2* in targeted lung cell populations, $Sox9^{Cre/+}$ lung distal epithelium, $Dermo^{Cre/+}$ or $Pdgfra^{Cre/+}$ lung mesenchyme all resulted in postnatal or perinatal lethality (Zhang et al., 2020). Although inducible systems such as doxycycline (tTA and rtTA) and tamoxifen-inducible CreERT/loxP offer an alternative way to enable gene manipulation in a temporally or spatially controlled manner to prevent lethality due to early or global ablation or overexpression, this system involves complex animal breeding strategies (Rawlins and Perl, 2012). Thus, direct administration of TAT-Cre protein in tissue slices provides a simple, rapid, cost and time-effective way of achieving temporally controlled gene manipulation directly in *ex vivo* tissue.

Another advantage is that numerous PCLS (~100 PCLS) can be generated from the lungs of a single adult transgenic floxed animal enabling untreated PCLS from the same animal to be incorporated into experiments that serve as a 'true' experimental controls, compared to the various littermate controls of different genotypes that are required for conventional Cre-Lox experiments. The ability to use controls from the same animal eliminates the potential introduction of confounding variables associated with using separate experimental and control animals. The TReATS method can also be used to vary the level of gene manipulation by applying TAT-Cre to PCLS from floxed heterozygous animals to induce single allelic gene alteration or floxed homozygotes for bi-allelic gene modification.

Furthermore, although spatial or temporal control of Cre expression using cell-type, tissue or developmental stage-specific promoters is possible, the prerequisite and limitation of this approach is the availability and specificity of relevant promoters (Kim et al., 2018; Rawlins and Perl, 2012). Tremendous progress has been made to establish different cell or tissue-specific promoters to restrict Cre expression in cells or tissues of interest (Kim et al., 2018; Rawlins and Perl, 2012). In addition, Cre driver lines that enable global deletion of floxed genes are available (Ramsbottom et

al., 2014; Schwenk et al., 1995). However, there are currently no organ-specific promoters, i.e. Cre driver lines that can simultaneously induce recombination of floxed alleles in all cell types or tissues within a single organ whereas the TReATS method can achieve this.

Nonetheless, the TReATS method described here is not without its limitations. One limitation is the viability of PCLS over time, in culture. In this study, we maintained the PCLS up to 96 h without significant reduction in cell viability. Other studies have shown viable PCLS for up to 8 days in culture (Alsafadi et al., 2020; Michalaki et al., 2022). If prolonged culture of PCLS is required to observe long term effects of gene ablation or overexpression, embedding PCLS in hydrogel has been shown to effectively extend their viability for at least 3 weeks (Bailey et al., 2020).

In the current study, we validated the loss of functional VANGL2 protein following TAT-Cre recombinase treatment of *Vangl2*$^{flox/flox}$ PCLS by showing characteristic disrupted F-actin distribution in Cre-treated *Vangl2*$^{flox/flox}$ PCLS. Disorganisation of the actin cytoskeleton is a hallmark of *Vangl2* dysfunction that has previously been demonstrated in both *Vangl2* LOF mouse models and following siRNA knockdown of *VANGL2* in cells (Cheong et al., 2020; Poobalasingam et al., 2017; Yates et al., 2010). Cre-mediated recombination was assessed by qRT-PCR of the gene of interest (Fig. 1D and 3B) and visualisation of EYFP protein expression by fluorescence microscopy (Fig. 1B, 2A-E). An alternative option to assess the efficiency of *Vangl2* allele recombination would have been to evaluate VANGL2 protein levels either by immunostaining or Western blot, however it is very challenging to obtain VANGL2 protein data due to a lack of effective and/or specific antibodies (Belotti et al., 2012) but this is a viable alternative to evaluate recombination efficiency of other targets of interest. In future, flow cytometry could be explored as an alternative to immunostaining for validation and quantification of Cre-mediated recombination efficiencies in tissue slices (Michalaki et al., 2022).

The novel strategy, TReATS (TAT-Cre Recombinase-mediated floxed Allele modification in Tissue Slices) described in this manuscript combines two powerful technologies: PCTS and cell-permeant Cre. TReATS provides a rapid and highly effective gene manipulation solution in *ex vivo* tissue slices, which has not been possible thus far. The establishment of this method constitutes a major advance in the use of PCTS and is anticipated to greatly expand their utility for research and drug screening purposes.

MATERIALS AND METHODS

Mice

All animal maintenance and procedures were conducted in compliance with the requirements of the Animal (Scientific Procedures) Act 1986. Animal work was approved by the South Kensington AWERB committee at Imperial College London. Mice were housed in specific pathogen-free conditions and given food and water *ad libitum*. Wild-type mice were purchased from Charles River (United Kingdom), *R26R-EYFP* mice, previously described (Srinivas et al., 2001), were kindly gifted by Dr Luis Tiago (Imperial College London) and *Vangl2*$^{flox/flox}$ and *Vangl2*$^{Lp/+}$ mice were supplied by Medical Research Council (MRC) Harwell (Oxford, United Kingdom). *R26R-EYFP*, *Vangl2*$^{flox/flox}$ *and Vangl2*$^{Lp/+}$ mouse strains were genotyped using previously described methods (Ramsbottom et al., 2014; Srinivas et al., 2001; Strong and Hollander, 1949). The structure of floxed alleles in *R26R-EYFP* and *Vangl2*$^{flox/flox}$ are illustrated in Fig. 1A and Fig. 3A, respectively. *Vangl2*$^{Lp/+}$ mice carry a heterozygous missense mutation S464N that results in VANGL2 LOF (Kibar et al., 2001; Murdoch, 2001). Wild-type, *R26R-EYFP* and *Vangl2*$^{flox/flox}$ were maintained on a C57BL/6J background, whereas *Vangl2*$^{Lp/+}$ mice were of C3H/HeH strain. Male or female adult mice aged 10–20 weeks were used in this study. *R26R-EYFP* (n = 4), *Vangl2*$^{Lp/+}$ (n = 4), wild-type (n = 3), and *Vangl2*$^{flox/flox}$ (n =1) were used in this study. All experiments were run in triplicate.

Precision-cut lung slices (PCLS) generation and culture

PCLS were generated from wild-type, *R26R-EYFP*, *Vangl2*$^{flox/flox}$ and *Vangl2*$^{Lp/+}$ adult mouse lungs as previously described with slight modifications (Akram et al., 2019b). Briefly, adult mice were humanely culled using intraperitoneal injection with pentobarbital. The anterior chest and neck wall were removed. A small incision was made in the anterior wall of the trachea just below the cricoid cartilage. A 21G rigid metal cannula was inserted into the incision and the lungs were inflated by injecting 1.2-1.5 ml of 2% (w/v) low-gelling temperature agarose (Sigma–Aldrich; Cat# A9414) dissolved in 1× Hank's Balanced Salt Solution (HBSS; Life Technology; Cat# 14025-100) containing 1% 4-(2-hydroxyethyl)-1-piper-azineethanesulfonic acid (HEPES) buffer (Life Technology; Cat# 15630080). After inflation, agarose was solidified by applying ice to the chest cavity. The lungs and heart were then excised from the body and immediately submerged in ice-cold HBSS/HEPES buffer and kept on ice until slicing.

Individual lung lobes were carefully separated and cut transversely at 250 µm using an automated vibratome (Compresstome VF-300-0Z; Precisionary Instruments LLC). Slices were generated in ice-cold HBSS/HEPES buffer and were transferred to 48-well plates containing ice-cold serum-free (SF) DMEM (Sigma; Cat# 31966021) with 1% penicillin-streptomycin (Merck; Cat# P0781). PCLS were generated from the central 2/3^{rds} of the lobe to ensure consistency in size. PCLS were then incubated overnight at 37◦C in 5% CO_2 and washed three times with warm SF-DMEM to remove excess agarose before use in experiments.

Cell-permeant TAT-Cre recombinase treatment

PCLS generated from *R26R-EYFP* mouse lungs were incubated with 3 µM of TAT-Cre recombinase (Merck; Cat# SCR508) in SF-DMEM for 24 h at 37◦C in 5% CO_2. After 24 h of incubation, TAT-Cre recombinase solution was removed and fresh SF-DMEM medium was added and incubated at 37◦C in 5% CO_2 for further 48 h. For *Vangl2*$^{flox/flox}$, 5 µM of TAT-Cre recombinase was added and PCLS were left submerged in the TAT-Cre solution for 72 h. Untreated, control PCLS from the same mouse were used as a negative control for each experiment. PCLS from wild-type mice with matched C57BL/6J background were treated with 5 µM of TAT-Cre recombinase and used as a negative control.

Live staining of PCLS and confocal imaging

At 72 h post-Cre treatment, PCLS from *R26R-EYFP* were immunolabelled with markers specific to key alveolar cell types using conjugated antibodies. Briefly, PCLS were incubated for 2 h at 37◦C in the dark with Alexa Fluor® 647-conjugated rat anti-LAMP3 (Dendritics; Cat# DDX0192A647; 1:250), podoplanin eFluor® 660 (Life Technologies; Cat# 50-5381-82; 1:500), Alexa Fluor® 647-conjugated PECAM (Biolegend; Cat# 102416; 1:200), Alexa Fluor® 647-conjugated CD11c (Biolegend; Cat# 117312; 1:200), or BioTracker™ TiY Vimentin Live Cell Dye (Sigma-Aldrich; Cat# SCT059; 1:2,000) diluted in SF-DMEM (antibody and cell dye details are shown in Table S1). Cell nuclei were labelled with DAPI (Life Technologies; Cat# 62248; 1:500) during the last 15 minutes of antibody incubation. To validate the absence of any non-specific binding of the conjugated fluorophores employed in live-cell imaging, PCLS were stained with appropriate isotype IgG control antibodies: Armenian hamster IgG-PE (Biolegend; Cat# 400907) for TiY Vimentin or rat IgG-Alexa Fluor 647 (Biolegend; Cat# 400526) for LAMP3, PDPN, PECAM, and CD11c, at 1:200 for 2 h at 37◦C and counterstained with DAPI as above. PCLS were then washed three

times with warm phenol red-free SF-DMEM (Life Technologies; Cat# 21063029) and immediately used for live imaging. PCLS from *R26R-EYFP* PCLS were placed into uncoated Ibidi 24-well µ-plates (Ibidi; Cat# 82421) and held in place by 6.5 mm Transwell® with 0.4 µm pores (Scientific Laboratory Supplies; Cat# 3470) as previously described (Akram et al., 2019b). PCLS were imaged on a Leica SP8 inverted confocal microscope using a HC PL APO 10×/0.40 air objective lens or HC PL APO 40×/1.30 oil objective lens.

To generate Z-stack images, TAT-Cre recombinase-treated *R26R-EYFP* PCLS were transferred into an Ibidi 8-well chamber microscopy slide (Ibidi; Cat# 80826) and labelled with DAPI for 15 minutes at 37◦C. PCLS were then washed with phenol red-free SF-DMEM and incubated with ProLong™ Live Antifade Reagent (Invitrogen; Cat# P36975; 1:100 dilution in phenol red-free SF-DMEM) for 15 minutes to prevent fluorophore bleaching during the imaging process. Excessive ProLong™ Live Antifade solution was removed, only droplets of Antifade solution was retained in the chamber slide to immobilise PCLS and ensure that the PCLS were kept moist throughout the imaging process. A total of 126 images were captured along the Z-plane of the PCLS (Z = 125 µm; 1 µm step size) on a Leica SP8 inverted confocal microscope using a HC PL APO 40×/1.30 oil objective lens. For some images, channel colours were changed during image post-processing for optimal data visualisation.

Immunofluorescence and confocal imaging

PCLS from *Vangl2*$^{flox/flox}$, *Vangl2*$^{Lp/+}$ and wild-type mice were fixed with 4% (v/v) paraformaldehyde (PFA) for 15 min at room temperature (RT), washed three times in PBS, permeabilised with 0.5% Triton X-100 in PBS at RT for 30 min, followed by 1 h blocking with PBSBT (1% BSA, 0.2% Triton X-100 in PBS) at RT. After blocking, PCLS were incubated with mouse anti-pan-cytokeratin (Sigma–Aldrich; Cat# C2931; 1:200) diluted in PBSBT blocking buffer at 4◦C overnight. After three washes in PBSBT, PCLS were then incubated with Rhodamine Phalloidin (Biotium; Cat# 00027; 1:200) and goat anti-mouse IgG (H+L) Alexa Fluor 647 secondary antibody (Thermo Fisher Scientific; Cat# 21235; 1:500) at RT for 2 h (antibody details are shown in Table S1). After washing in PBS, cell nuclei were labelled with DAPI (Sigma Aldrich; Cat# D9542; 1:500). Coverslips were then mounted with ProLong™ Gold Antifade Mountant (Invitrogen; Cat# P36930). PCLS were imaged on a Leica SP8 inverted confocal microscope using a HC PL APO 40×/1.30 oil objective lens. For some

images, channel colours were changed during image post-processing for optimal data visualisation.

RNA extraction and quantitative real-time PCR (qRT-PCR)

PCLS homogenisation was carried out using a FastPrep-24^{TM} Tissue Homogeniser (MP Biomedicals) followed by total RNA extraction from PCLS using the RNeasy mini kit (Qiagen) according to the manufacturer's protocols. Each RNA sample was produced from pooling three PCLS and three RNA samples were prepared for each condition per experiment. RNA concentration and quality were assessed using the TapeStation 2200 (Agilent). Only samples with RNA integrity number (RIN) value > 8 were used for cDNA conversion and subsequent qRT-PCR. Approximately 200 ng of total RNA was reverse-transcribed to cDNA using the High-Capacity cDNA Reverse Transcription kit (Applied Biosystems) according to manufacturer's instructions. Quantitative RT-PCR was performed using TaqMan Fast Advanced Master Mix (Life Technologies) and run on a 7500 Fast Real-Time PCR system (Applied Biosystems). *B2m* was used as a reference gene. Relative transcript levels were analysed using the $2^{-\Delta\Delta CT}$ method. Four *R26R-EYFP* and one *Vangl2*$^{flox/flox}$ mice were used and all samples were tested in triplicate. All primers used in this study were purchased from Life Technologies as follows: *B2m* (Mm00437762_m1), *Vangl2* (Mm00473768_m1), and *YFP* (Mr04097229_mr).

MTT Assay

MTT assay (Roche; Cat. No 11465007001) was performed according to manufacturer's instructions to assess cell viability at the end point of TAT-Cre recombinase experiments. Briefly, PCLS of equal size were placed into 48-well plates, one slice per well. 250 µl of 10% MTT solution in SF-DMEM was added into each well and incubated at 37◦C for 45 minutes. MTT solution was then discarded and 250 µl of DMSO was added to solubilise the formazan crystals that formed within the viable cells and incubated for 10 min at 37◦C. 200 µl of eluted formazan solution from each well was then transferred to a 96-well plate and absorbance (OD) was measured at 570 nm and 690 nm using a SpectraMax® iD3 microplate reader (Molecular Devices). PCLS treated with 70% methanol were used as positive control for dead cells with no metabolic activity, whereas untreated, control PCLS were used as positive controls with normal metabolic activity. MTT assay was performed in triplicate for each condition.

Statistical analysis

All graphs and statistical tests were produced in GraphPad Prism 8. Data are presented as mean ± the standard error of the mean (SEM). Comparisons of multiple groups were performed using a Kruskal-Wallis test with Dunn's multiple comparison post-test. Datasets comparing two groups were analysed using a Mann-Whitney U test. 'p' values of <0.05 were considered statistically significant. Details of the statistical tests used, the value of n, and number of experiments performed are detailed in the figure legends.

Acknowledgments

We thank the Mary Lyon Centre, MRC Harwell and The Central Biomedical Services (CBS) animal facility at Imperial College London South Kensington campus for excellent animal husbandry. We also thank the Facility for Imaging by Light Microscopy (FILM) at Imperial College London for microscopy support. Infrastructure support for this research was provided by the NIHR Imperial Biomedical Research Centre (BRC).

Competing interests

The authors declare no competing interests.

Funding

This project was funded by the Royal Brompton and Harefield Hospitals Charity (grant number: 123 P90719) and an award from Mr. and Mrs Youssef Mansour. T.C.L was supported by a Sir Henry Dale Fellowship from the Wellcome Trust and The Royal Society (210424/Z/18/Z).

Author contributions

S-S.C. and C.H.D designed the research; S-S.C. conducted the experiments and analysed the data; S-S.C. and C.H.D wrote the paper. T.C.L. provided and genotyped *R26R-EYFP* mice. M.S and R.H provided and genotyped *Vangl2*$^{flox/flox}$ and *Vangl2*$^{Lp/+}$ mice. M.H and C.H.D acquired the funding. All authors discussed the results and manuscript.

References

Akram, K. M., Yates, L.L., Mongey, R., Rothery, S., Gaboriau, D.C., Sanderson, J., Hind, M., Griffiths, M. and, and Dean, C.H. (2019a). Time-lapse Imaging of Alveologenesis in Mouse Precision-cut Lung Slices. Bio-protocol 9, e3403.

Akram, Khondoker M., Yates, L.L., Mongey, R., Rothery, S., Gaboriau, D.C.A., Sanderson, J., Hind, M., Griffiths, M., and Dean, C.H. (2019b). Live imaging of alveologenesis in precision-cut lung slices reveals dynamic epithelial cell behaviour. Nat. Commun. 10.

Alsafadi, H.N., Staab-Weijnitz, C.A., Lehmann, M., Lindner, M., Peschel, B., Königshoff, M., and Wagner, D.E. (2017). An ex vivo model to induce early fibrosis-like changes in human precision-cut lung slices. Am. J. Physiol. - Lung Cell. Mol. Physiol. 312, L896–L902.

Alsafadi, H.N., Uhl, F.E., Pineda, R.H., Bailey, K.E., Rojas, M., Wagner, D.E., and Konigshoff, M. (2020). Applications and Approaches for Three-Dimensional Precision-Cut Lung Slices. Am. J. Respir. Cell Mol. Biol. 62, 681–691.

Bailey, K.E., Pino, C., Lennon, M.L., Lyons, A., Jacot, J.G., Lammers, S.R., Konigshoff, M., and Magin, C.M. (2020). Embedding of precision-cut lung slices in engineered hydrogel biomaterials supports extended ex vivo culture. Am. J. Respir. Cell Mol. Biol. 62, 14–22.

Belotti, E., Puvirajesinghe, T.M., Audebert, S., Baudelet, E., Camoin, L., Pierres, M., Lasvaux, L., Ferracci, G., Montcouquiol, M., and Borg, J.P. (2012). Molecular Characterisation of Endogenous Vangl2/Vangl1 Heteromeric Protein Complexes. PLoS One 7.

Branda, C.S., and Dymecki, S.M. (2004). Talking about a Revolution: The Impact of Site-Specific Recombinases on Genetic Analyses in Mice Review. Dev. Cell 6, 7–28.

Bryson, K.J., Garrido, D., Esposito, M., McLachlan, G., Digard, P., Schouler, C., Guabiraba, R., Trapp, S., and Vervelde, L. (2020). Precision cut lung slices: A novel versatile tool to examine host-pathogen interaction in the chicken lung. Vet. Res. 51, 1–16.

Bugeon, S., De Chevigny, A., Boutin, C., Coré, N., Wild, S., Bosio, A., Cremer, H., and Beclin, C. (2017). Direct and efficient transfection of mouse neural stem cells and mature neurons by in vivo mRNA electroporation. Dev. 144, 3968–3977.

Byrne, A.J., Mathie, S.A., Gregory, L.G., and Lloyd, C.M. (2015). Pulmonary macrophages: Key players in the innate defence of the airways. Thorax 70, 1189–1196.

Cheong, S.S., Akram, K.M., Matellan, C., Kim, S.Y., Gaboriau, D.C.A., Hind, M., del Río Hernández, A.E., Griffiths, M., and Dean, C.H. (2020). The Planar Polarity Component VANGL2 Is a Key Regulator of Mechanosignaling. Front. Cell Dev. Biol. 8, 1–21.

De Graaf, I.A.M., Olinga, P., De Jager, M.H., Merema, M.T., De Kanter, R., Van De Kerkhof, E.G., and Groothuis, G.M.M. (2010). Preparation and incubation of precision-cut liver and intestinal slices for application in drug metabolism and toxicity studies. Nat. Protoc. 5, 1540–1551.

De Kanter, R., Monshouwer, M., Draaisma, A.L., De Jager, M.H., De Graaf, I.A.M., Proost, J.H., Meijer, D.K.F., and Groothuis, G.M.M. (2004). Prediction of whole-body metabolic clearance of drugs through the combined use of slices from rat liver, lung, kidney, small intestine and colon. Xenobiotica 34, 229–241.

DeLisser, H.M., Helmke, B.P., Cao, G., Egan, P.M., Taichman, D., Fehrenbach, M., Zaman, A., Cui, Z., Mohan, G.S., Baldwin, H.S., et al. (2006). Loss of PECAM-1 function impairs alveolarization. J. Biol. Chem. 281, 8724–8731.

Denk, F., Ramer, L.M., Erskine, E.L.K.S., Nassar, M.A., Bogdanov, Y., Signore, M., Wood, J.N., McMahon, S.B., and Ramer, M.S. (2015). Tamoxifen induces cellular stress in the nervous system by inhibiting cholesterol synthesis. Acta Neuropathol. Commun. 3, 74.

Fuhrmann-Benzakein, E., García-Gabay, I., Pepper, M.S., Vassalli, J.D., and Herrera, P.L. (2000). Inducible and irreversible control of gene expression using a single transgene. Nucleic Acids Res. 28, 3–7.

Geoffroy, C.G., and Raineteau, O. (2007). A Cre-lox approach for transient transgene expression in neural precursor cells and long-term tracking of their progeny in vitro and in vivo. BMC Dev. Biol. 7, 1–15.

Gitton, Y., Tibaldi, L., Dupont, E., Levi, G., and Joliot, A. (2009). Efficient CPP-mediated Cre protein delivery to developing and adult CNS tissues. BMC Biotechnol. 9.

Guillot, L., Nathan, N., Tabary, O., Thouvenin, G., Le Rouzic, P., Corvol, H., Amselem, S., and Clement, A. (2013). Alveolar epithelial cells: Master regulators of lung homeostasis. Int. J. Biochem. Cell Biol. 45, 2568–2573.

Hubrecht, R.C., and Carter, E. (2019). The 3Rs and humane experimental technique: Implementing change. Animals 9, 1–10.

Kauffman, K.J., Oberli, M.A., Dorkin, J.R., Hurtado, J.E., Kaczmarek, J.C., Bhadani, S., Wyckoff, J., Langer, R., Jaklenec, A., and Anderson, D.G. (2018). Rapid, Single-Cell Analysis and Discovery of Vectored mRNA Transfection In Vivo with a loxP-Flanked tdTomato Reporter Mouse. Mol. Ther. - Nucleic Acids 10, 55–63.

Kibar, Z., Vogan, K.J., Groulx, N., Justice, M.J., Underhill, D.A., and Gros, P. (2001). Ltap, a mammalian homolog of Drosophila Strabismus/Van Gogh, is altered in the mouse neural tube mutant Loop-tail. Nat. Genet. 28, 251–255.

Kim, H., Kim, M., Im, S.-K., and Fang, S. (2018). Mouse Cre-LoxP system: general principles to determine tissue-specific roles of target genes. Lab. Anim. Res. 34, 147.

Kim, Y.S., Mongey, R., Wang, P., Rothery, S., David, C., Gaboriau, A., Hind, M., Griffiths, M., and Dean, C.H. (2021). The acid injury and repair (AIR) model : A novel ex-vivo tool to understand lung repair. Biomaterials 267.

Krumdieck, C.L., dos Santos, J., and Ho, K.-J. (1980). A new instrument for the rapid preparation of tissue slices. Anal. Biochem. 104, 118–123.

Laresgoiti, U., Niko, M.Z., Rao, C., Brady, J.L., Richardson, R. V., Batchen, E.J., Chapman, K.E., and Rawlins, E.L. (2016). Lung epithelial tip progenitors integrate glucocorticoid- and STAT3-mediated signals to control progeny fate. Dev. 143, 3686–3699.

Majorova, D., Atkins, E., Martineau, H., Vokral, I., Oosterhuis, D., Olinga, P., Wren, B., Cuccui, J., and Werling, D. (2021). Use of Precision-Cut Tissue Slices as a Translational Model to Study Host-Pathogen Interaction. Front. Vet. Sci. 8, 1–7.

Marconett, C.N., Zhou, B., Sunohara, M., Pouldar, T.M., Wang, H., Liu, Y., Rieger, M.E., Tran, E., Flodby, P., Siegmund, K.D., et al. (2017). Cross-species transcriptome profiling identifies new alveolar epithelial Type i Cell-specific genes. Am. J. Respir. Cell Mol. Biol. 56, 310–321.

Michalaki, C., Dean, C., and Johansson, C. (2022). The Use of Precision-Cut Lung Slices for Studying Innate Immunity to Viral Infections 1–19.

Misharin, A. V., Morales-Nebreda, L., Mutlu, G.M., Budinger, G.R.S., and Perlman, H. (2013). Flow cytometric analysis of macrophages and dendritic cell subsets in the mouse lung. Am. J. Respir. Cell Mol. Biol. 49, 503–510.

Morimoto, M., Liu, Z., Cheng, H.T., Winters, N., Bader, D., and Kopan, R. (2010). Canonical Notch signaling in the developing lung is required for determination of arterial smooth muscle cells and selection of Clara versus ciliated cell fate. J. Cell Sci. 123, 213–224.

Murdoch, J.N. (2001). Severe neural tube defects in the loop-tail mouse result from mutation of Lpp1, a novel gene involved in floor plate specification. Hum. Mol. Genet. 10, 2593–2601.

Närhi, K., Nagaraj, A.S., Parri, E., Turkki, R., van Duijn, P.W., Hemmes, A., Lahtela, J., Uotinen, V., Mäyränpää, M.I., Salmenkivi, K., et al. (2018). Spatial aspects of oncogenic signalling determine the response to combination therapy in slice explants from Kras-driven lung tumours. J. Pathol. 245, 101–113.

Oishi, I., Suzuki, H., Onishi, N., Takada, R., Kani, S., Ohkawara, B., Koshida, I., Suzuki, K., Yamada, G., Schwabe, G.C., et al. (2003). The receptor tyrosine kinase Ror2 is involved in non-canonical Wnt5a/JNK signalling pathway. Genes to Cells 8, 645–654.

Ou, Q., Jacobson, Z., Abouleisa, R.R.E., Tang, X.L., Hindi, S.M., Kumar, A., Ivey, K.N., Giridharan, G., El-Baz, A., Brittian, K., et al. (2020). Physiological Biomimetic Culture System for Pig and Human Heart Slices. Circ. Res. 628–642.

Pai, K.S., and Ravindranath, V. (1991). Protection and potentiation of MPTP-induced toxicity by cytochrome P-450 inhibitors and inducer: in vitro studies with brain slices. Brain Res. 555, 239–244.

Peitz, M., Pfannkuche, K., Rajewsky, K., and Edenhofer, F. (2002). Ability of the hydrophobic FGF and basic TAT peptides to promote cellular uptake of recombinant Cre recombinase: A tool for efficient genetic engineering of mammalian genomes. Proc. Natl. Acad. Sci. U. S. A. 99, 4489–4494.

Placke, M.E., and Fisher, G.L. (1987). Adult peripheral lung organ culture--a model for respiratory tract toxicology. Toxicol. Appl. Pharmacol. 90, 284–298.

Poobalasingam, T., Yates, L.L., Walker, S.A., Pereira, M., Gross, N.Y., Ali, A., Kolatsi-Joannou, M., Jarvelin, M.-R., Pekkanen, J., Papakrivopoulou, E., et al. (2017). Heterozygous Vangl2 Looptail mice reveal novel roles for the planar cell polarity pathway in adult lung homeostasis and repair. Dis. Model. Mech. 10, 409–423.

Ramsbottom, S.A., Sharma, V., Rhee, H.J., Eley, L., Phillips, H.M., Rigby, H.F., Dean, C., Chaudhry, B., and Henderson, D.J. (2014). Vangl2-Regulated Polarisation of Second Heart Field-Derived Cells Is Required for Outflow Tract Lengthening during Cardiac Development. PLoS Genet. 10.

Rawlins, E.L., and Perl, A.K. (2012). The a"MAZE"ing world of lung-specific transgenic mice. Am. J. Respir. Cell Mol. Biol. 46, 269–282.

Rohlmann, A., Gotthardt, M., Willnow, T.E., Hammer, R.E., and Herz, J. (1996). Sustained somatic gene inactivation by viral transfer of Cre recombinase. Nat. Biotechnol. 14, 1562–1565.

Ruigrok, M.J.R., Maggan, N., Willaert, D., Frijlink, H.W., Melgert, B.N., Olinga, P., and Hinrichs, W.L.J. (2017). siRNA-Mediated RNA Interference in Precision-Cut Tissue Slices Prepared from Mouse Lung and Kidney. AAPS J. 19, 1855–1863.

Ryder, E., Doe, B., Gleeson, D., Houghton, R., Dalvi, P., Grau, E., Habib, B., Miklejewska, E., Newman, S., Sethi, D., et al. (2014). Rapid conversion of EUCOMM/KOMP-CSD alleles in mouse embryos using a cell-permeable Cre recombinase. Transgenic Res. 23, 177–185.

Sanghvi-Shah, R., and Weber, G.F. (2017). Intermediate filaments at the junction of mechanotransduction, migration, and development. Front. Cell Dev. Biol. 5, 1–19.

Savery, D., Maniou, E., Culshaw, L.H., Greene, N.D.E., Copp, A.J., and Galea, G.L. (2020). Refinement of inducible gene deletion in embryos of pregnant mice. Birth Defects Res. 112, 196–204.

Schwenk, F., Baron, U., and Rajewsky, K. (1995). A cre-transgenic mouse strain for the ubiquitous deletion of loxP-flanked gene segments including deletion in germ cells. Nucleic Acids Res. 23, 5080–5081.

Srinivas, S., Watanabe, T., Lin, C.S., William, C.M., Tanabe, Y., Jessell, T.M., and Costantini, F. (2001). Cre reporter strains produced by targeted insertion of EYFP and ECFP into the ROSA26 locus. BMC Dev. Biol. 1, 1–8.

Strong, L.., and Hollander, W.. (1949). Hereditary Looptail in the house mouse. J. Hered. 40, 329–334.

Surolia, R., Li, F.J., Wang, Z., Li, H., Dsouza, K., Thomas, V., Mirov, S., Pérez-Sala, D., Athar, M., Thannickal, V.J., and Antony, V.B. (2019). Vimentin intermediate filament assembly regulates fibroblast invasion in fibrogenic lung injury. JCI Insight 4, 1–17.

Van Den Plas, D., Ponsaerts, P., Van Tendeloo, V., Van Bockstaele, D.R., Berneman, Z.N., and Merregaert, J. (2003). Efficient removal of LoxP-flanked genes by electroporation of Cre-recombinase mRNA. Biochem. Biophys. Res. Commun. 305, 10–15.

White, E.S. (2015). Lung extracellular matrix and fibroblast function. Ann. Am. Thorac. Soc. 12, S30–S33.

Yates, L.L., Papakrivopoulou, J., Long, D.A., Goggolidou, P., Connolly, J.O., Woolf, A.S., and Dean, C.H. (2010). The planar cell polarity gene Vangl2 is required for mammalian kidney-branching morphogenesis and glomerular maturation. Hum. Mol. Genet. 19, 4663–4676.

Yin, H., Copley, C.O., Goodrich, L. V., and Deans, M.R. (2012). Comparison of phenotypes between different vangl2 mutants demonstrates dominant effects of the looptail mutation during hair cell development. PLoS One 7.

Zhang, K., Yao, E., Lin, C., Chou, Y., Wong, J., Li, J., Wolters, P.J., Chuang, P., and States, U. (2020). A mammalian Wnt5a – Ror2 – Vangl2 axis controls the cytoskeleton and confers cellular properties required for alveologenesis. Elife 9, e53688.

Figures

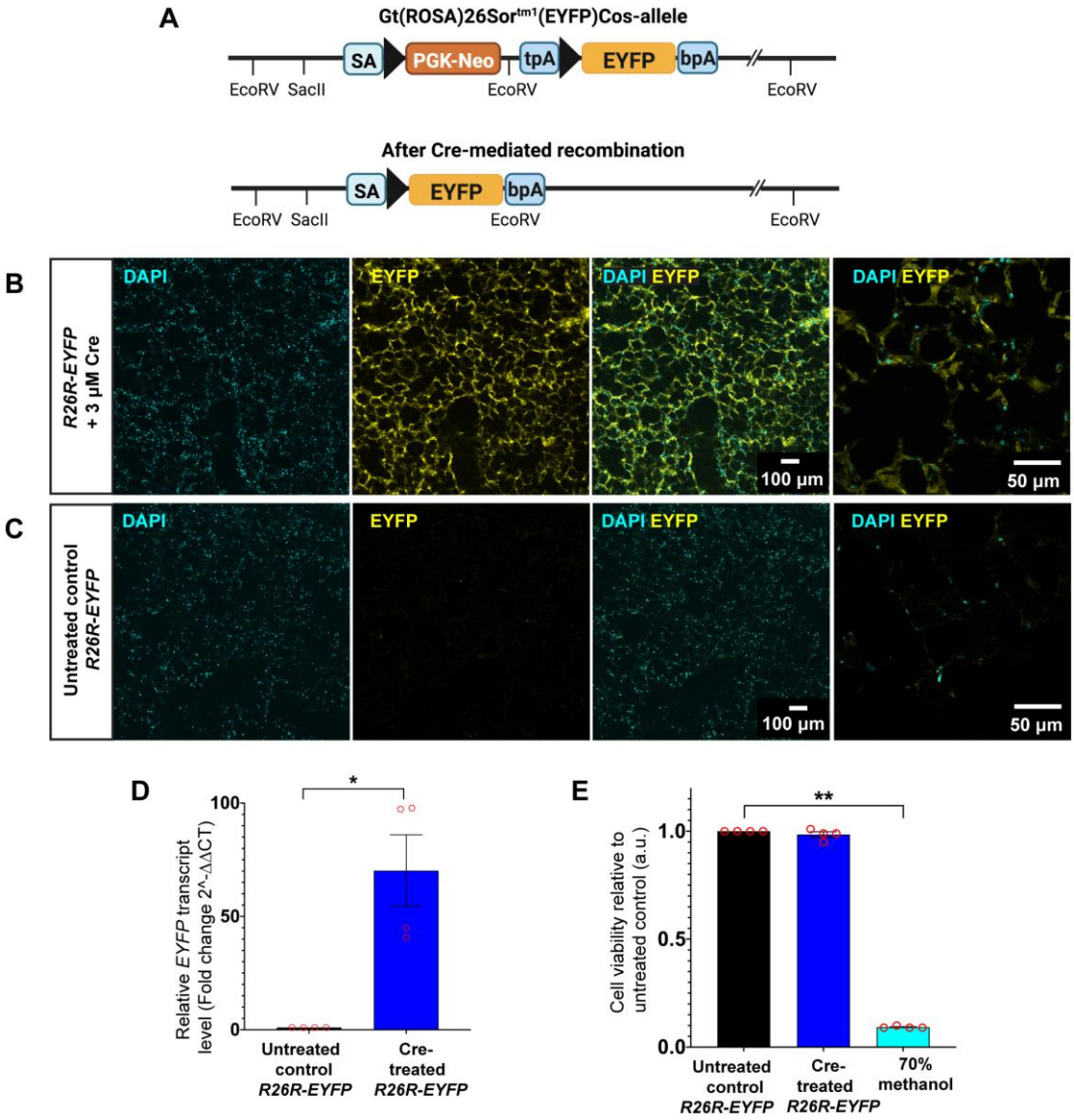

Fig. 1. TAT-Cre recombinase induces recombination of *loxP*-modified alleles and activates EYFP expression in PCLS from adult *R26R-EYFP* mice. (A) Schematic showing the structure of *loxP*-modified allele in *R26R-EYFP* mice, and the structure of the targeted locus after Cre-mediated excision of the *loxP*-flanked (PGK-neo selective marker and a tpA transcriptional stop sequence) cassette. *EYFP* is localised downstream of the *lox-P* flanked cassette. *LoxP* sites are indicated by solid black arrowheads. **(B)** Representative images showing TAT-Cre recombinase-treated *R26R-EYFP* PCLS and **(C)** untreated control *R26R-EYFP* PCLS analysed by fluorescence microscopy. EYFP protein expression is shown in yellow and cell nuclei were labelled with DAPI (cyan); n = 4 mice; three PCLS per condition per experiment. Images were captured on a confocal microscope using a HC PL APO 10×/0.40 air

objective lens. **(D)** Histogram shows transcript levels for *EYFP* in untreated control and TAT-Cre recombinase-treated *R26R-EYFP* PCLS; n = 4 mice, three PCLS were pooled for each RNA sample, three RNA samples per condition per experiment, each experiment was run in triplicate. Data are presented as mean ± SEM; Mann–Whitney *U*-test, *$p < 0.05$. **(E)** Assessment of cell viability using MTT assay for untreated control and TAT-Cre recombinase-treated *R26R-EYFP* PCLS. PCLS treated with 70% methanol serves as a positive control for dead cells. n = 4 mice, each experiment was run in triplicate. Data are presented as mean ± SEM; Kruskal–Wallis with Dunn's multiple comparisons test, **$p < 0.01$.

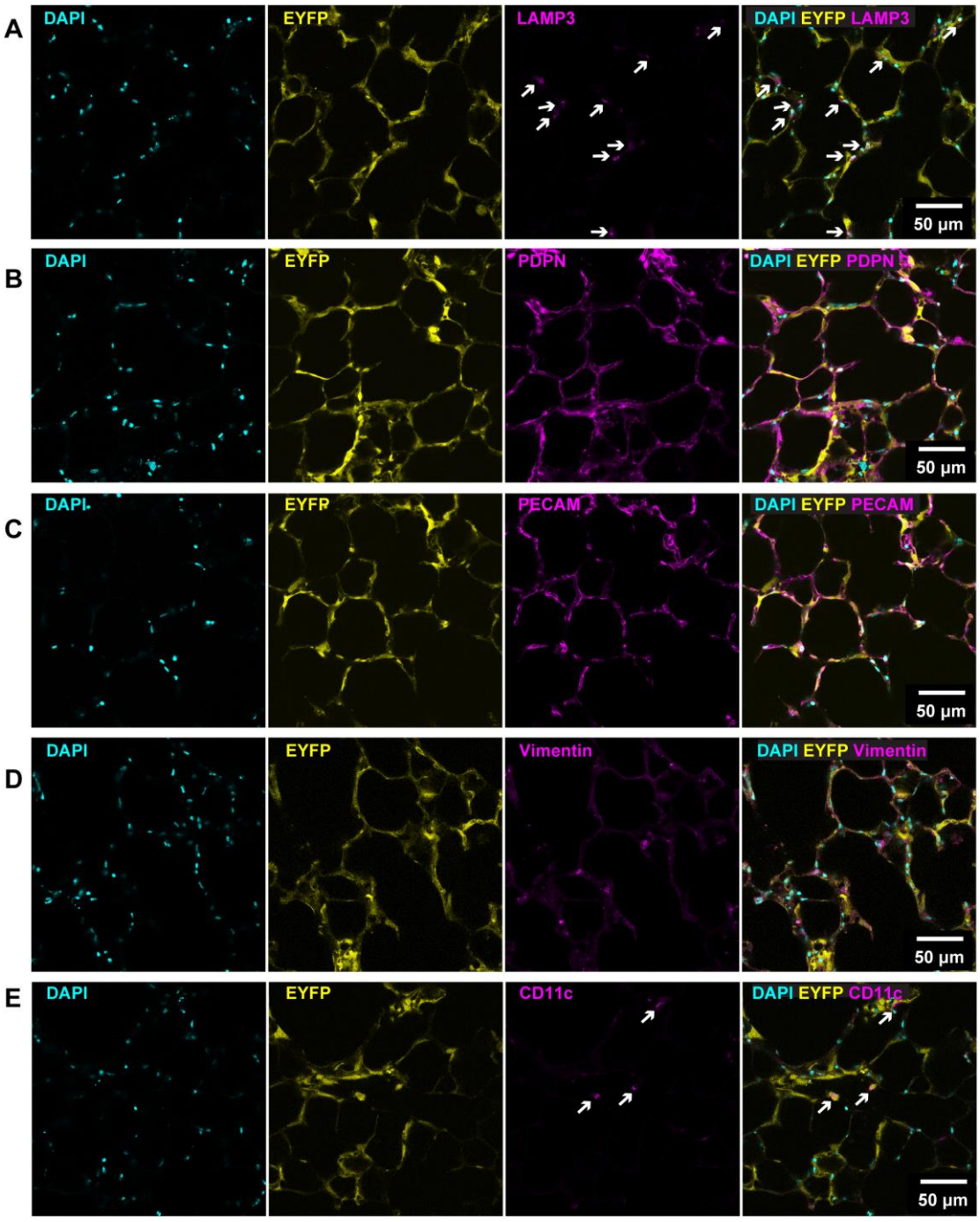

Fig. 2. TAT-Cre recombinase induces EYFP expression in key alveolar cell types. Representative images showing co-localisation of EYFP (yellow) with LAMP3^{+} differentiated cuboidal alveolar type 2 (AT2) epithelial cells (magenta; indicated by white arrows) **(A),** podoplanin (PDPN)$^{+}$ alveolar type 1 (AT1) epithelial cells (magenta) **(B)**, PECAM^{+} endothelial cells (magenta) **(C)**, vimentin^{+} fibroblast cells (magenta) **(D),** and CD11c^{+} macrophages (magenta; indicated by white arrows) **(E)** in TAT-Cre recombinase-treated *R26R-EYFP* PCLS. Images were captured on a confocal microscope using a HC PL APO 40×/1.30 oil objective lens. Cell nuclei were labelled with DAPI (cyan); n = 4 mice, each experiment was run in triplicate.

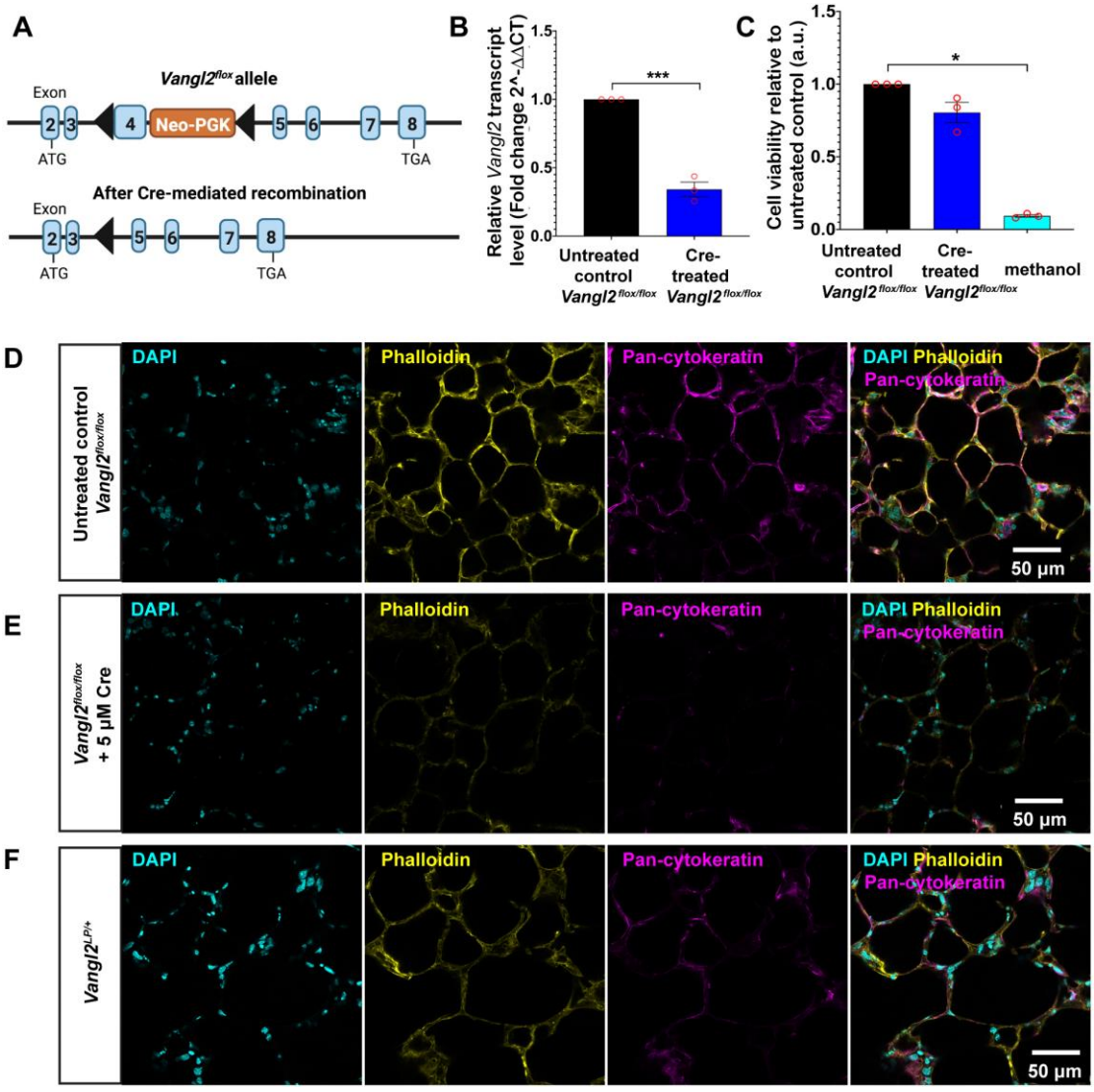

Fig. 3. TAT-Cre recombinase treatment induces *Vangl2* deletion in adult *Vangl2*$^{flox/flox}$ mouse PCLS. **(A)** Schematic showing the structure of *loxP*-modified allele in *Vangl2*$^{flox/flox}$ transgenic, and the structure of the targeted locus after Cre-mediated excision of the *loxP*-flanked exon 4 of the *Vangl2* gene. Deletion of exon 4 leads to loss of the critical transmembrane domains of VANGL2 protein. *LoxP* sites are indicated by solid black arrowheads. **(B)** Histogram shows transcript levels for *Vangl2* in untreated control and TAT-Cre recombinase-treated *Vangl2*$^{flox/flox}$ PCLS using primers flanking exon 3-4 boundary of the *Vangl2* gene; n = 1 mouse, three PCLS were pooled for each RNA sample, three RNA samples per condition per experiment, each experiment was run in triplicate. Data are presented as mean ± SEM; Two-tailed unpaired Student's *t*-test, ***$p < 0.001$. **(C)** Assessment of cell viability using MTT assay for untreated control and TAT-Cre recombinase-treated *Vangl2*$^{flox/flox}$ PCLS. PCLS treated with 70% methanol was used as a positive control

for dead cells. n = 1 mouse, each experiment was run in triplicate. Data are presented as mean ± SEM; Kruskal–Wallis with Dunn's multiple comparisons test, *$p < 0.05$. **(D-F)** Labelling of F-actin (Phalloidin; yellow) and immunofluorescence staining for intermediate filaments (pan-cytokeratin; magenta) in untreated control *Vangl2*$^{flox/flox}$ PCLS **(D)**, TAT-Cre recombinase-treated *Vangl2*$^{flox/flox}$ PCLS **(E)**, and heterozygous *Vangl2*$^{Lp/+}$ PCLS **(F)**. Images were captured on a confocal microscope using a HC PL APO 40×/1.30 oil objective lens. Nuclei were stained with DAPI (cyan).

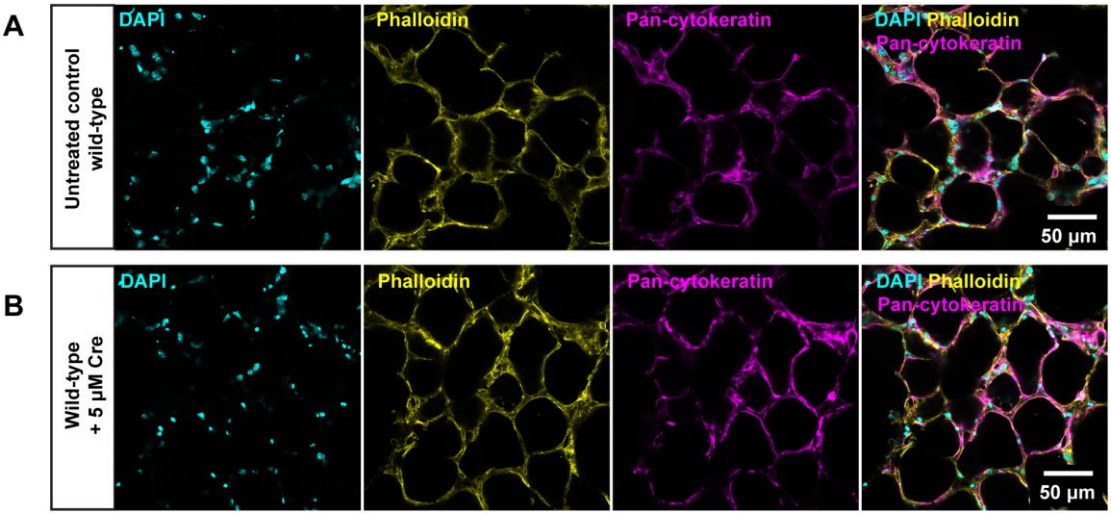

Fig. 4. F-actin and intermediate filament phenotype in wild-type control PCLS. (A-B) Labelling of F-actin (Phalloidin; yellow) and immunofluorescence staining for intermediate filaments (pan-cytokeratin; magenta) in untreated control wild-type PCLS **(A)**, and TAT-Cre recombinase-treated wild-type PCLS **(B)**. Images were captured on a confocal microscope using a HC PL APO 40×/1.30 oil objective lens. Nuclei were stained with DAPI (cyan). n = 3 mice, each experiment was run in triplicate.

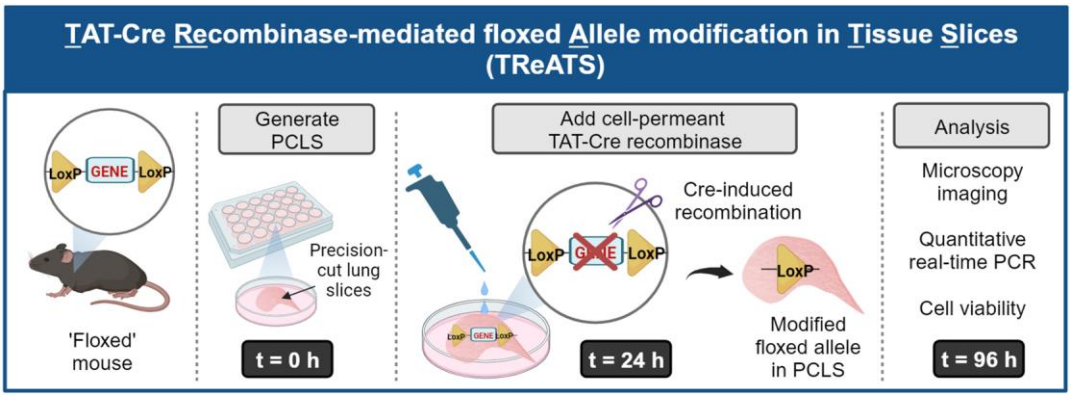

Fig. 5. The experimental flow of TAT-Cre Recombinase-mediated floxed Allele modification in Tissue Slices (TReATS). PCLS are generated from transgenic mouse carrying floxed allele(s) of interest and maintained in DMEM culture media. At t = 24 h, TAT-Cre recombinase is added and PCLS are incubated in TAT-Cre solution for 72 h. At the end point (t = 96 h), microscopy imaging and quantitative real-time PCR are performed to assess recombination efficiency. Cell viability test is conducted to determine cell metabolic activity of PCLS. Diagram was created with BioRender.

Table S1. List of antibodies and cell dyes used in this study.

Primary Antibodies	Host	Conjugation	Dilution	Supplier	Reference
LAMP3	Rat	Alexa Fluor® 647	1:250	Dendritics	DDX0192A647
Podoplanin	Syrian hamster	eFluor™ 660	1:500	Life Technologies	50-5381-82
PECAM	Rat	Alexa Fluor® 647	1:200	Biolegend	102416
CD11c	Armenian hamster	Alexa Fluor® 647	1:200	Biolegend	117312
Pan-Cytokeratin	Mouse	Unconjugated	1:200	Sigma-Aldrich	C2931
Cell dyes	**Host**	**Conjugation**	**Dilution**	**Supplier**	**Reference**
Vimentin	NA	TiY	1:2,000	Sigma-Aldrich	SCT059
Phalloidin	NA	Rhodamine	1:200	Biotium	00027
Secondary Antibodies	**Host**	**Conjugation**	**Dilution**	**Supplier**	**Reference**
α-mouse	Goat	Alexa Fluor® 647	1:500	Thermo Fisher Scientific	21235
IgG isotype control	Armenian hamster	PE	1:200	Biolegend	400907
IgG isotype control	Rat	Alexa Fluor® 647	1:200	Biolegend	400526

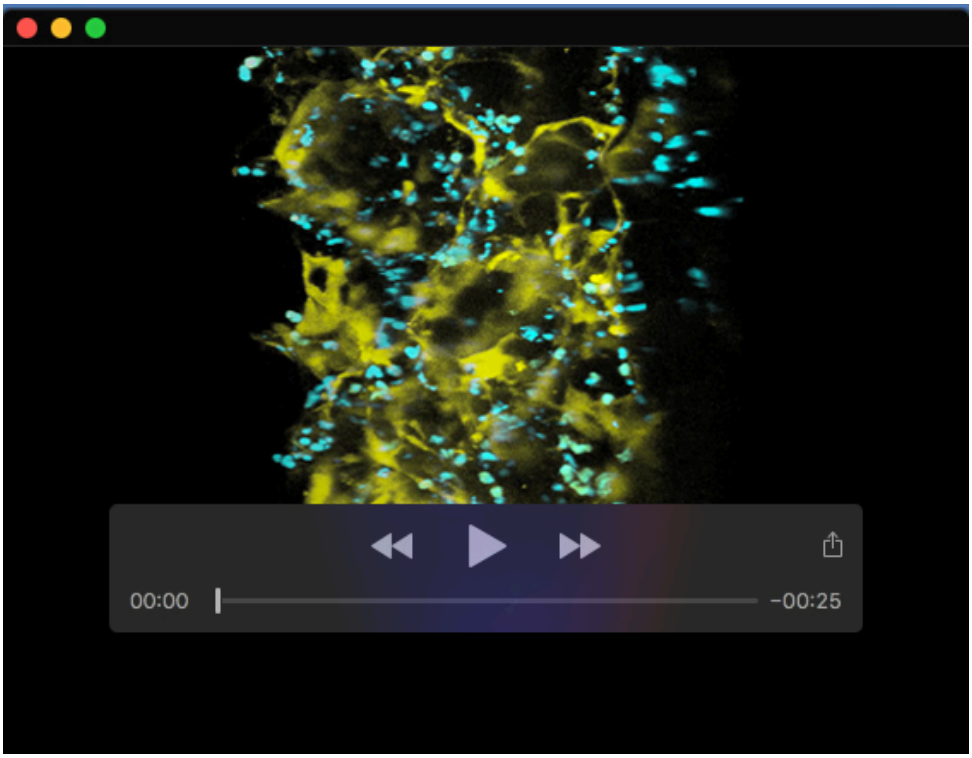

Movie 1. Video showing 3D projection of *R26R-EYFP* PCLS treated with TAT-Cre recombinase. A total of 126 Z-slices were acquired with 1 µm step size, reaching a depth of 125 µm. EYFP and DAPI signals are visualised as peak brightest point, rotating on the Y-axis. Images were captured on a confocal microscope using a HC PL APO 40×/1.30 oil objective lens (working distance = 0.24 mm). EYFP is shown in yellow and cell nuclei were counterstained with DAPI (cyan).

Disease Models & Mechanisms • Supplementary information